Dalton Transactions

Accepted Manuscript

ROYAL SOCIETY OF CHEMISTRY

www.rsc.org/dalton

Journal Name

ARTICLE

Double-decker bis(tetradiazepinoporphyrazinato) rare earth complexes: crucial role of intramolecular hydrogen bonding

Received 00th January 20xx,
Accepted 00th January 20xx

DOI: 10.1039/x0xx00000x

www.rsc.org/

Ekaterina N. Tarakanova,*[a] Stanislav A. Trashin,[a] Anton O. Simakov,[b] Taniyuki Furuyama,[c] Alexander V. Dzuban,[d] Liana N. Inasaridze,[e] Pavel A. Tarakanov,[a] Pavel A. Troshin,[e] Victor E. Pushkarev,[a] Nagao Kobayashi[c,‡] and Larisa G. Tomilova[a,d]

A series of homoleptic bis{tetrakis(5,7-bis(4-*tert*-butylphenyl)-6*H*-1,4-diazepino)[2,3-*b*,*g*,*l*,*q*]porphyrazinato} lanthanide sandwich complexes [$^{t\text{BuPh}}$DzPz]$_2$Ln (Ln = Lu, Er, Dy, Eu, Nd, Ce, La) were prepared and their physicochemical properties were studied to gain insight into the nature of specific interactions in diazepinoporphyrazines. The effect of annulated diazepine moieties and Ln ionic radius on the properties of the complexes was investigated in comparison to double-decker phthalocyanines. A combination of experimental and theoretical studies revealed the presence of two types of hydrogen bonding interactions in the metal-free porphyrazine and the corresponding sandwich complexes, namely, interligand C–H^{ax}…N^{meso} hydrogen bonding and O–H…N^{Dz} ligand–water interaction. The interligand hydrogen bonding imparts the high stability of the ligand dimer and the double-decker compounds in reduced state. This work is the first comprehensive investigation into fundamental understanding of unusual properties of diazepine-containing macroheterocycles.

Introduction

Phthalocyanines (Pcs) are commonly known synthetic tetraazaporphyrinoids with excellent thermal and chemical stability. Owing to an impressive variety of functional properties, these remarkable chromophores possess numerous applications in catalysis, photonics, electronics and medicine.[1-4] An important class of Pc analogs with nonplanar π-extended system includes seven-membered ring-fused porphyrazines, specifically diazepinoporphyrazines. Since the discovery of diazepinoporphyrazines in 1999[5], these macroheterocyclic molecules have attracted significant interest due to their unique structural features and unusual physicochemical properties.[6-10]

Intrinsic spectral properties of diazepinoporphyrazines, such as Q-band splitting in the UV-vis spectra of their metal complexes, were initially thought to be associated with n-π* transitions caused by lone-pair electrons of the nitrogen atoms in the diazepine ring(s).[5-7] However, recent studies challenged this concept and showed that specific properties of diazepinoporphyrazines can result from the formation of stable dimers.[11-13] Nevertheless, the nature of interligand interactions in diazepinoporphyrazines still remains unclear. Conversely, sandwich-type tetrapyrrole rare earth (REE) complexes, in particular bis(Pcs), represent prime examples of compounds whose spectral properties are determined by the extent of intramolecular π-π interactions.[14] Jiang and co-workers developed a common theory that helps to understand the structure-property relationship for this class of molecules.[14-17] Consequently, double-decker Pc derivatives, which are being actively investigated as promising materials for sensing devices, optoelectronics and spintronics,[14-16, 18-29] can serve as ideal model systems to study the character of interligand interactions.

Recently, we reported the first examples of tetradiazepinoporphyrazine-based sandwich-type lanthanide complexes and assumed the presence of additional intramolecular interactions between the macrocycles.[30-32] To shed light on the nature of the specific interactions in diazepinoporphyrazines, herein we provide the first comprehensive study on a series of sandwich double-decker tetradiazepinoporphyrazine lanthanide compounds including a detailed experimental characterization and theoretical study of the corresponding free-base porphyrazine. Insights into self-assembly of the complexes are provided, which can be further exploited in future work.

[a] *Institute of Physiologically Active Compounds, Russian Academy of Sciences, 1 Severny proezd, 142432 Chernogolovka, Moscow Region, Russian Federation. E-mail: tarakanova.ek.nik@gmail.com*
[b] *Centre for Theoretical and Computational Chemistry (CTCC), Department of Chemistry, University of Oslo, P. O. Box 1033 Blindern, N-0315 Oslo, Norway*
[c] *Department of Chemistry, Graduate School of Science, Tohoku University, Sendai 980-8578, Japan*
[d] *Department of Chemistry, M.V. Lomonosov Moscow State University, 1 Leninskie Gory, 119991 Moscow, Russian Federation. E-mail: tom@org.chem.msu.ru*
[e] *Institute for Problems of Chemical Physics, Russian Academy of Sciences, 1 Semenov Prospect, 142432 Chernogolovka, Moscow region, Russian Federation*

† Electronic Supplementary Information (ESI) available: HRMS data, 1D and 2D NMR spectra, results of DOSY experiments, additional UV-Vis spectroscopic data, results of DLS measurements for **2a** and **2d**, detailed description of the thermal analysis data, CV of **2b**, **2c**, **2e**, SWVA of **2a–g**, full computational details. See DOI: 10.1039/x0xx00000x

Experimental section

Chemicals and instrumentation. Lanthanide acetylacetonates $Ln(acac)_3$ were prepared according to the reported method[33] and dried under high vacuum for 4 h at 50 °C prior to use. All other reagents and solvents were purchased from Sigma-Aldrich and used as received. When necessary, solvents were purified following standard procedures. Analytical thin layer chromatography (TLC) was performed on ALUGRAM® Alox N/UV_{254} aluminum oxide precoated sheets (Macherey-Nagel). Size exclusion column chromatography was carried out using Bio-Beads S-X1 resin (BIORAD) eluted with CH_2Cl_2.

Electronic absorption spectra were recorded on Hitachi U-2900 (UV-vis) and Hitachi U-4100 (UV-vis-NIR) spectrophotometers. Matrix-assisted laser desorption/ionization time-of-flight (MALDI-TOF) mass spectra were acquired on a VISION-2000 mass spectrometer with α-cyano-4-hydroxycinnamic acid (CHCA) as the matrix. High-resolution MALDI mass spectra were recorded on a Bruker Ultraflex II TOF/TOF instrument with CHCA as the matrix. ^{1}H NMR, ^{13}C NMR, ^{1}H-^{1}H COSY, ^{1}H-^{13}C HSQC, ^{1}H-^{13}C HMQC and ^{1}H-^{13}C NOESY spectra were collected on a Bruker Avance 500 spectrometer (500 MHz) with samples dissolved in CD_2Cl_2 at 22 °C, unless otherwise specified. Chemical shifts are given in parts per million (ppm) relative to TMS ($SiMe_4$). Dynamic light scattering (DLS) measurements were performed using a Photocor Complex particle size analyzer. The electron spin resonance (ESR) spectra were recorded on a Benchtop ESR spectrometer Adani CMS8400 at 25 °C.

Cyclic voltammetry (CV) and square-wave voltammetry (SWV) were conducted in a conventional three-electrode cell with Pt-disk (2.0 mm in diameter) working and Pt-foil counter electrodes. The saturated calomel reference electrode (SCE) was connected to the solution through a salt bridge, and the junction potential of the reference electrode was corrected to a ferrocenium$^+$/ferrocene (Fc^+/Fc) reference pair. *o*-Dichlorobenzene (*o*-DCB, 99% SigmaAldrich, HPLC-grade), freshly passed through an Al_2O_3 layer, was used as the solvent, and 0.15 M $[Bu_4N][BF_4]$ ($TBABF_4$, Sigma-Aldrich, dried under vacuum at 80 °C) was used as the supporting electrolyte. The sample solution (1–5 x 10^{-4} M) was purged with nitrogen for at least 20 min before measurements were taken. The scan rate in the CV measurements was varied from 0.02 to 1.00 V s^{-1}. A frequency of 10 Hz and an amplitude potential of 0.05 V were used for SWV. All measurements were performed at ambient temperature (22 ± 1 °C).

Field-emission scanning electron microscopy (FE-SEM) was carried out using a Hitachi SU8000 high resolution microscope. Images were acquired in secondary electron mode with a 0.7 kV accelerating voltage and 4–5 mm working distance. A target-oriented approach was utilized for the optimization of the analytic measurements.[34] Before measurements, the samples were mounted on a 25 mm aluminum specimen stub and fixed by conductive silver paint. Sample morphology was studied under native conditions to exclude metal coating surface effects.[35]

Thermoanalytical investigations were carried out on an STA 409 PC Luxx (Netzsch) simultaneous thermal analyzer coupled with a QMS 403C Aëolos quadrupole mass spectrometer. Measurements were performed in an alumina crucible within a temperature range of 40–1000 °C (heating rate 10 °C min^{-1}) under an argon or air atmosphere.

Magnetic circular dichroism (MCD) spectra were collected on a JASCO J-725 spectrodichrometer equipped with a JASCO electromagnet that produces magnetic fields of up to 1.03 T (Tesla) with both parallel and antiparallel fields, and its magnitudes were expressed in terms of molar ellipticity per tesla ($[\theta]_M$/deg M^{-1} cm^{-1} T^{-1}).

All quantum chemical calculations were performed with the ORCA electronic structure program[36] using the standard generalized gradient approximation (GGA) functional BP86. Ahlrichs split-valence def2-SV(P) basis set[37] was used on first- and second-row elements, while the relativistic small-core Stuttgart/Dresden effective core potentials (ECPs), which replace 28 core electrons SD(28,MWB) and the corresponding valence basis sets using a segmented contraction scheme SD(28,MWB)-SEG, was used for lanthanides.[38] To significantly speed up the calculations, the resolution of identity (RI) approximation,[39, 40] also known as the density fitting approximation, was exploited. For the first- and second-row elements described by the Ahlrichs def2-SV(P) basis set, the corresponding well-tested Weigend auxiliary def2-SVP/J basis set[41] was used while for lanthanides the auxiliary basis set was constructed automatically by the ORCA program. Dispersion forces were taken into account by the DFT-D3 atom-pairwise dispersion corrections with Becke-Johnson damping developed by Grimme and co-workers.[42, 43] Calculations for open shell lanthanide complexes were done using the spin unrestricted formalism. Default DFT integration grids were used: Grid2 (a pruned Lebedev-110 grid) for the SCF iterations and Grid4 (a pruned Lebedev-302 grid) during the final energy evaluation after the SCF convergence. Tight SCF and geometry optimization convergence criteria were used; no symmetry constraints were imposed during the geometry optimization. For ligand dimers, harmonic vibrational frequencies were calculated analytically to verify that a geometry optimization has found a true potential energy minimum and not a saddle point. The Natural bond orbital (NBO) analysis of Weinhold and co-workers was done using the stand-alone NBO 6.0 executable.[44]

Synthesis of tetrakis(5,7-bis(4-*tert*-butylphenyl)-6*H*-1,4-diazepino)[2,3-b,g,l,q]porphyrazine (1). Ligand **1** was synthesized according to the previously described procedure[30] and exists in the dimeric form (see the Supporting Information).

General procedure for the preparation of double-deckers 2a–g ($[^{tBuPh}DzPz]_2Ln$). A mixture of ligand **1** (0.031 mmol) and $Ln(acac)_3$ (0.017 mmol) was dissolved in dry *o*-DCB (3 mL), and 1,8-diazabicyclo[5.4.0]undec-7-ene (DBU, 46 mg, 0.31 mmol) was then added. The solution was refluxed and stirred for 1.5–3.5 h under an argon atmosphere until the complete disappearance of the starting ligand. The course of the reaction was monitored by TLC (Al_2O_3, CH_2Cl_2:THF 20:1 V/V)

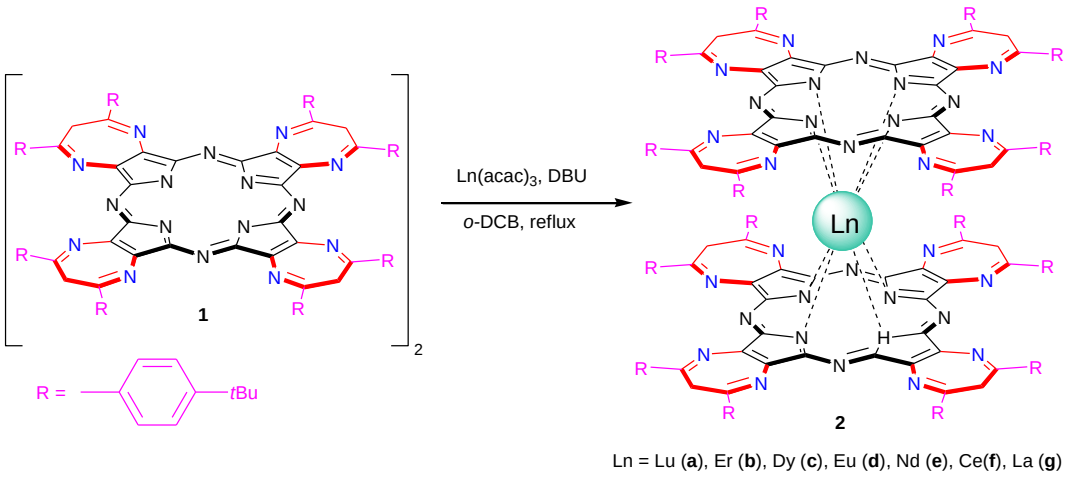

Ln = Lu (**a**), Er (**b**), Dy (**c**), Eu (**d**), Nd (**e**), Ce(**f**), La (**g**)

Scheme 1 The synthesis of double-decker complexes **2a–g**.

and UV-vis spectroscopy. After the removal of the solvent under reduced pressure, the residue was washed with 80% aqueous MeOH (4 × 50 mL) and dried under high vacuum. The crude product was purified by gel permeation column chromatography (Bio-Beads S-X1, CH_2Cl_2) to give the title compound **2** as a bluish-green solid.

Bis{tetrakis(5,7-bis(4-*tert*-butylphenyl)-6*H*-1,4-diazepino)[2,3-*b,g,l,q*]porphyrazinato} lutetium (2a). UV-vis (CH_2Cl_2) λ_{max}/nm (log ε): 369 (5.09), 620 (4.86), 722 (4.78). ^{1}H NMR (500 MHz; CD_2Cl_2) δ/ppm: 7.99 (32H, br s, $H^{o\text{-}Ar}$), 7.48 (32H, br s, $H^{m\text{-}Ar}$), 6.02 (8H, br s, H^{eq}), 5.13 (8H, br s, H^{ax}), 1.50 (144H, s, H^{tBu}). ^{13}C NMR (500 MHz; CD_2Cl_2) δ/ppm: 154.2, 149.7, 142.1, 134.8, 129.8, 126.1, 39.2, 35.4, 31.6. MS (MALDI-TOF/TOF; HCCA): *m/z* 3444.775 $[M+H]^+$; calculated for $C_{216}H_{226}LuN_{32}$: 3444.814.

Bis{tetrakis(5,7-bis(4-*tert*-butylphenyl)-6*H*-1,4-diazepino)[2,3-*b,g,l,q*]porphyrazinato} erbium (2b). UV-vis (CH_2Cl_2) λ_{max}/nm: 368 (5.12), 621 (4.89), 714 (4.80). ^{1}H NMR (500 MHz; CD_2Cl_2) δ/ppm: 21.20 (32H, br s, $H^{o\text{-}Ar}$), 14.24 (32H, br s, $H^{m\text{-}Ar}$), 33.75 (8H, br s, H^{eq}), 67.44 (8H, br s, H^{ax}), 5.51 (144H, s, H^{tBu}). MS (MALDI-TOF/TOF; HCCA): *m/z* 3436.963 $[M+H]^+$; calculated for $C_{216}H_{226}ErN_{32}$: 3436.805.

Bis{tetrakis(5,7-bis(4-*tert*-butylphenyl)-6*H*-1,4-diazepino)[2,3-*b,g,l,q*]porphyrazinato} dysprosium (2c). UV-vis (CH_2Cl_2) λ_{max}/nm: 367 (5.24), 628 (4.91), 707 (4.85). ^{1}H NMR (500 MHz; CD_2Cl_2) δ/ppm: -17.29 (32H, br s, $H^{o\text{-}Ar}$), -5.43 (32H, br s, $H^{m\text{-}Ar}$), -45.83 (8H, br s, H^{eq}), -113.08 (8H, br s, H^{ax}), -6.20 (144H, s, H^{tBu}). MS (MALDI-TOF/TOF; HCCA): *m/z* 3433.047 $[M+H]^+$; calculated for $C_{216}H_{226}DyN_{32}$: 3432.801.

Bis{tetrakis(5,7-bis(4-*tert*-butylphenyl)-6*H*-1,4-diazepino)[2,3-*b,g,l,q*]porphyrazinato} europium (2d). UV-vis (CH_2Cl_2) λ_{max}/nm (log ε): 368 (5.20), 631 (5.03), 699 (4.89). ^{1}H NMR (500 MHz; CD_2Cl_2) δ/ppm: 9.00 (32H, br s, $H^{o\text{-}Ar}$), 8.02 (32H, br s, $H^{m\text{-}Ar}$), 8.42 (8H, br s, H^{eq}), 10.01 (8H, br s, H^{ax}), 1.82 (144H, s, H^{tBu}). MS (MALDI-TOF/TOF; HCCA): *m/z* 3423.041 $[M+H]^+$; calculated for $C_{216}H_{226}EuN_{32}$: 3422.793.

Bis{tetrakis(5,7-bis(4-*tert*-butylphenyl)-6*H*-1,4-diazepino)[2,3-*b,g,l,q*]porphyrazinato} neodymium (2e). UV-vis (CH_2Cl_2) λ_{max}/nm: 367 (5.28), 634 (5.18), 687 (5.00). ^{1}H NMR (500 MHz; CD_2Cl_2) δ/ppm: 6.41 (32H, br s, $H^{o\text{-}Ar}$), 6.65 (32H, br s, $H^{m\text{-}Ar}$), 2.55 (8H, br s, H^{eq}), -2.94 (8H, br s, H^{ax}), 1.01 (144H, s, H^{tBu}). MS (MALDI-TOF/TOF; HCCA): *m/z* 3414.124 $[M+H]^+$; calculated for $C_{216}H_{226}NdN_{32}$: 3413.784.

Bis{tetrakis(5,7-bis(4-*tert*-butylphenyl)-6*H*-1,4-diazepino)[2,3-*b,g,l,q*]porphyrazinato} cerium (2f) was characterized in our previous paper.[32]

Bis{tetrakis(5,7-bis(4-*tert*-butylphenyl)-6*H*-1,4-diazepino)[2,3-*b,g,l,q*]porphyrazinato} lanthanum (2g). UV-vis (CH_2Cl_2) λ_{max}/nm (log ε): 370 (5.25), 637 (5.31), 673 (5.02). ^{1}H NMR (500 MHz; CD_2Cl_2) δ/ppm: 7.98 (32H, d, ^3J = 6 Hz, $H^{o\text{-}Ar}$), 7.47 (32H, d, ^3J = 7.3 Hz, $H^{m\text{-}Ar}$), 6.05 (8H, d, ^2J = 11.7 Hz, H^{eq}), 4.69 (8H, d, ^2J = 12.7 Hz, H^{ax}), 1.50 (144H, s, H^{tBu}). ^{13}C NMR (500 MHz; CD_2Cl_2) δ/ppm: 154.4, 154.3, 148.3, 142.4, 134.5, 129.9, 126.1, 37.9, 35.4, 31.6. MS (MALDI-TOF/TOF; HCCA): *m/z* 3409.169 $[M+H]^+$; calculated for $C_{216}H_{226}ErN_{32}$: 3408.779.

Results and discussion

Synthesis

In this study, we extended our previous work[30-32] and synthesized a series of double-decker complexes, including representatives of early, middle and late lanthanides (Scheme 1). Hitherto undescribed double-decker complexes of erbium (**2b**), dysprosium (**2c**) and europium (**2d**) were prepared and purified in the same manner as previously reported **2e,g**[31] (Scheme 1 and Table S1).

All compounds obtained were structurally characterized by high-resolution mass spectrometry, NMR and UV-vis-NIR spectroscopy. The MALDI-TOF/TOF mass spectra of **2a–g** clearly show an intense peak of a protonated molecular ion $[M+H]^+$ with precise isotopic pattern supplemented with fragmentation peaks of a weak intensity (Table S1 and Figs. S1–S7).

Notably, the formation of sandwich-type complexes **2a–g** took place under the relatively mild reaction conditions previously developed for the selective synthesis of lanthanide mono(Pcs).[45] Moreover, the corresponding early lanthanide double-deckers demonstrated high stability towards

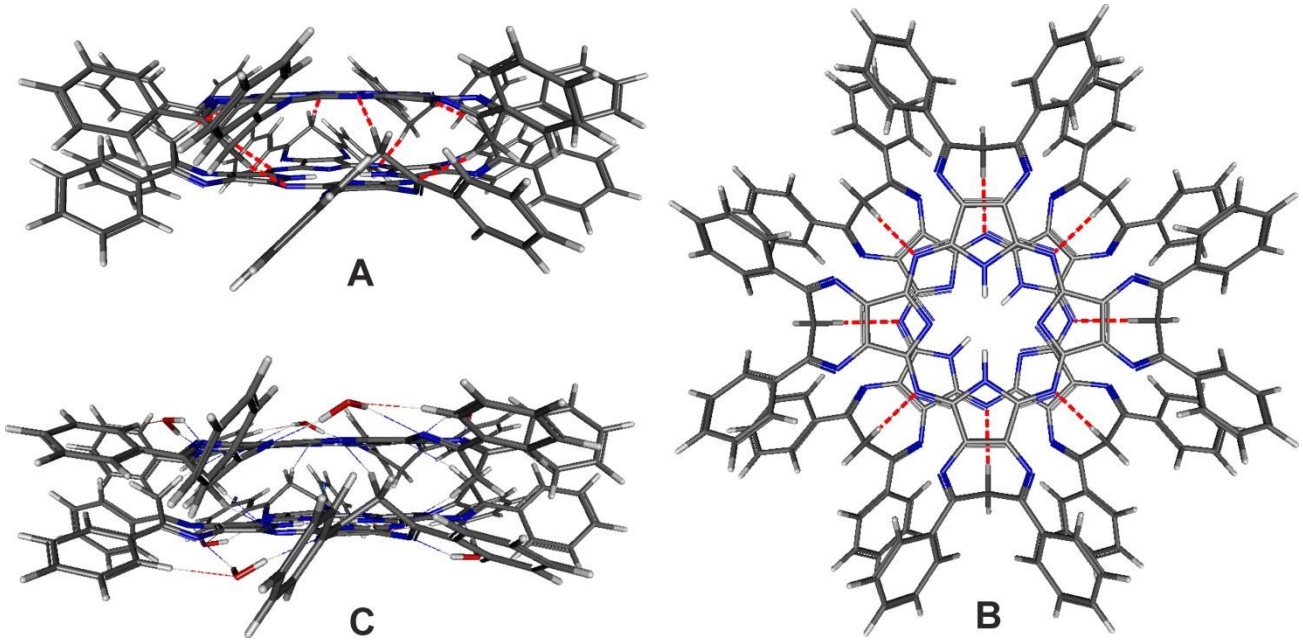

Fig. 1 DFT-optimized structures of the ligand dimer: (A) front view; (B) top view; (C) front view with water molecules incorporated. *Tert*-butyl substituents were omitted for shortening the calculation time.

dissociation as compared with Pc counterparts.[46-48] This suggested the presence of additional interligand interactions in tetradiazepinoporphyrazine lanthanide double-decker complexes provided by the diazepine moieties.

DFT study and NMR spectroscopy

To gain insight into the structural features of sandwich-type tetradiazepinoporphyrazine lanthanide complexes, we analyzed the structure of the free-base ligand and the double-decker compounds obtained using two-dimensional NMR techniques combined with quantum chemical calculations as discussed below. Although this approach assumes no comprehensive information about the atomic coordinates, it provides basic knowledge of the structure of compounds in solution.

Recently, it was shown that magnesium(II) tetradiazepinoporphyrazinate exists in the form of H-type dimer in solution in the absence of strong coordinating agents.[11, 12] Another study revealed that the complicated nature of the UV-vis spectrum of tribenzodiazepinoporphyrazine ligand, with three intense bands in the Q-band region, is due to propensity of this compound to form H- and J-type aggregates via intermolecular hydrogen bonds.[13] In this work, using a combination of diffusion-ordered NMR spectroscopy (DOSY) (Table S2), UV-vis and fluorescence experiments (Figs. S37–S41), we first demonstrated the existence of ligand **1** in dimeric form in solution. Furthermore, the ligand was found to retain dimeric structure regardless of the concentration (Figs. S40 and S41). Geometry optimization of the free-base ligand **1** at the BP86/def2-SV(P) level of theory further confirms the dimeric structure of **1**, leading exclusively to H-type dimer. The calculations also demonstrate the presence of the strong hydrogen bonding interactions, denoted as C–H^{ax}…N^{meso}, which involve diastereotopic protons at C6 position of diazepine rings, occupying an axial orientation (H^{ax}), and *meso*-nitrogen atoms (N^{meso}) of the adjacent macrocycle (Fig. 1).

NBO analysis revealed that hydrogen bonding between ligands in dimer **1** is formed by occupation of nonbonding molecular orbital (MO) localized predominantly at the C–H^{ax} bond of the one ligand with lone-pair electrons of the N^{meso} atom of the opposite ligand. The presence of eight hydrogen bonds along with π-stacking contributes to the stabilization of tetradiazepinoporphyrazine dimers as compared with Pc analogs, which exhibit only π-π stacking interactions.[2, 14] Of particular note is that the nonplanar structure of 1,4-diazepine heterocycle and its ability to change conformation through ring inversion and rotation of phenyl substituents[49] (Fig. 1A) serve as prerequisites for the formation of self-complementary dimeric structure of ligand **1** with inward orientation of the eight diazepine moieties (Fig. 1).

Hydrogen bonding and the unique complementary configuration of diazepine moieties provide the distance between the planes of ligand dimer **1** of 3.23 Å and rotation angle of 45°, which are comparable to those in double-decker lanthanide complexes **2** (3.21 Å for **2g**; 2.95 Å for **2a**) and meet the symmetry of the coordination sphere of the lanthanide center, i.e. square antiprism. Thus, the closeness of geometries of the ligand dimer (Fig. 1) and the lanthanide complex (Fig. 2) reduces the steric barrier to the formation of the double-decker compounds. This leads to a significant decrease in temperature required for the formation of lanthanide bis(tetradiazepinoporphyrazinates) (Scheme 1) down to the value at which selective synthesis of lanthanide mono(Pcs) occurs.[45] Given that the calculated distance between the macrocycles in La complex **2g** is 3.21 Å, which is less than that

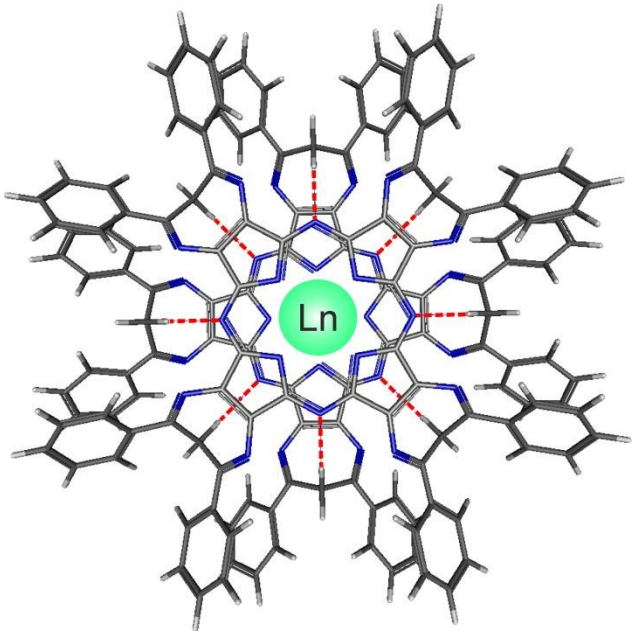

Fig. 2 DFT-optimized structure of the double-decker **2**.

in the ligand dimer (3.23 Å), the stability of the latter towards dissociation indicates a potential stability of **2g**, as described in earlier work.[31]

Moreover, the theoretical calculations (Figs. 1 and 2) suggest the propensity of macrocycles in lanthanide tetradiazepinoporphyrazine double-deckers, unlike Pc and porphyrin analogs, to preserve the mutual orientation with rotation angle close to 45°, regardless of the nature of lanthanide ion. This effect is of fundamental interest for the study of magnetic properties as a function of the symmetry of the coordination sphere of the lanthanide center.[50, 51]

As discussed below, double-deckers **2** contain water molecules in their structure. To evaluate the spatial position of water, its presence in ligand **1** near the centers of potential hydrogen bonding such as N^{meso} atoms of the macrocycle and nitrogen atoms of diazepine fragments (N^{Dz}) was simulated. Simulation showed that the most advantageous position of the water, while maintaining dimeric structure of the ligand, is close to the N^{Dz} atoms (Fig. 1C). Moreover, geometry optimization of the ligand dimer with water molecules initially localized between the planes of macrocycles near N^{meso} atoms led to displacement of water towards N^{Dz} atoms. In this case, hydrogen bonds O–H…N^{Dz}, each involving the protons of one water molecule and two N^{Dz} atoms of the adjacent diazepine fragments, are formed (Fig. 1C). Since the distance between the decks in each sandwich complex **2** is smaller compared to ligand dimer **1**, it can be assumed that water will be located outside the complexes near the N^{Dz} atoms as in the case of **1**.

Due to the stability of double-deckers **2a–e,g** in the anionic (reduced) form, denoted as $[^{tBuPh}DzPz]_2Ln^{III}H$, NMR spectra of reasonable quality were obtained (Figs. S8–S19) without the addition of reducing agents required in the case of REE bis(Pcs).[52, 53] Of special note is cerium complex **2f** which was isolated in a neutral diamagnetic form $[^{tBuPh}DzPz]_2Ce^{IV}$, incorporating Ln ion in the tetravalent oxidation state, as discussed recently.[32] Full assignment of proton signals in the NMR spectra was made using COSY and NOESY 2D NMR spectroscopy (Table 1 and Figs. S20–S36).

Table 1 ^{1}H NMR data (δ, ppm) for double-deckers **2a–g** in CD_2Cl_2

Compd	$H^{o\text{-}Ar}$	$H^{m\text{-}Ar}$	H^{eq}	H^{ax}	H^{tBu}	H^{H2O}
1	7.99	7.46	6.10	4.70	1.50	2.10–2.60
2a	7.99	7.48	6.02	5.13	1.50	2.70
2b	21.20	14.24	33.75	67.44	5.51	6.50
2c	-17.29	-5.43	-45.83	-113.08	-6.20	-7.00
2d	9.00	8.02	8.42	10.01	1.82	3.02
2e	6.41	6.65	2.55	-2.94	1.01	2.10
2f	8.05	7.52	6.18	5.13	1.52	2.34
2g	7.98	7.47	6.05	4.69	1.50	2.86

The ^{1}H NMR spectra of $[^{tBuPh}DzPz]_2Ln^{III}H$ containing paramagnetic Ln ions demonstrated characteristic lanthanide induced shifts (LIS) of the proton signals (Table 1) with the values dependent on both Ln nature and distance between Ln ion and the corresponding proton. Thus, Er and Eu (**2b** and **2d**, respectively) induce the downfield shift of the proton signals, while Dy and Nd (**2c** and **2e**, respectively) result in the upfield shift, with the highest LIS values characteristic for Er and Dy complexes. It is worth noting that in going from diamagnetic **2a** to paramagnetic **2b–e**, the equatorial protons at the C6 position of diazepine rings (H^{eq}) undergo a much stronger paramagnetic LIS compared with $H^{o\text{-}Ar}$ protons of phenyl rings despite the similar distance to the Ln ion. This is in good agreement with DFT optimized geometry of the sandwich complexes, where all diazepine rings in the macrocycles have the uniform conformation in which the diastereotopic protons are directed to the Ln ion. It should also be noted that the LIS effect was also observed in the case of H_2O protons, which indicates the involvement of water molecules in the sandwich structure. Small values of this shift (Table 1) imply insignificant influence of Ln paramagnetic effect due to the shielding of the Ln center by ^{tBuPh}DzPz macrocycles according to the DFT calculations (Fig. 1C). The position of water predicted by the calculations is further supported by the strongest NOESY correlation, and thus shortest distance, between H_2O protons and $H^{o\text{-}Ar}$ protons of phenyl rings (Figs. S24, S30, and S36).

Electronic absorption spectra

The UV-vis behavior of complexes **2a–g** agrees with their double-decker structure. The spectra generally correspond to classical REE bis(Pcs)[54-56] but also exhibit additional features. As is well known, Pc double-decker complexes predominantly exist as the neutral π-radical forms.[19, 55, 57] Unlike bis(Pcs), the isolated double-deckers **2a–g** exist in the anionic form $[^{tBuPh}DzPz]_2Ln^{III}H$ (Fig. 3), except for cerium compound **2f** which was isolated in the neutral diamagnetic form $[^{tBuPh}DzPz]_2Ce^{IV}$ owing to metal-centered Ce^{III}/Ce^{IV} oxidation, as reported recently.[32] The anionic forms can be chemically oxidized at the ligand side, e.g. by treatment with molecular iodine or bromine, giving the corresponding neutral form $[^{tBuPh}DzPz]_2Ln^{III}$

Table 2 UV-Vis-NIR data for double-deckers **2a–g** in CH_2Cl_2

Compd	λ_{max}, nm (log ε)						
	reduced state $[^{tBuPh}DzPz]_2Ln^{III}H$			neutral state $[^{tBuPh}DzPz]_2Ln^{III}$			
	B(Soret)	Q_1	Q_2	B(Soret)	Q	RV	IV[a]
2a	369(5.09)	620(4.86)	722(4.78)	342sh, 377	599sh, 653(5.00)	865(3.91)	1216sh, 1305
2b	368(5.12)	621(4.89)	714(4.8)	344sh, 377	601sh, 654(5.02)	861	1222sh, 1334
2c	367(5.24)	628(4.91)	707(4.85)	346sh, 379	601sh, 656(5.05)	857	1214sh, 1351, 1427sh
2d	368(5.20)	631(5.03)	699(4.89)	349sh, 380	602sh, 660(5.13)	853	1195sh, 1376sh, 1476
2e	346sh, 367(5.28)	634(5.18)	687(5.00)	363	607sh, 664(5.20)	846	1577
2f[b]	344sh, 371(5.30)	635(5.34)	678(5.03)	-	-	-	-
2g	350sh, 373(5.25)	638(5.31)	674(5.02)	365	610sh, 671(5.25)	839	1780

[a] The spectra were recorded in CCl_4. [b] The data are given for the reaction mixture.

(Fig. S42). Note that in the UV-vis spectra of the neutral forms of **2a–g** the characteristic π-radical blue valence (BV) band at 450–500 nm is poorly defined owing to absorption of diazepine moieties in this region. The π-radical nature of the neutral forms is confirmed by the presence of red valence (RV) and intervalence (IV) absorption bands in the NIR region (Fig. 4), whose line-shape and position correlate with the nature of REE. Table 2 summarizes all UV-vis-NIR data.

The presence of an unpaired electron in the neutral forms of the complexes $([L^{2-}Ln^{3+}L^{\cdot-}]^0$, where L = $^{tBuPh}DzPz)$ is also supported by the ESR spectroscopy. Intense ESR signal with a g-factor value of 2.0022 was observed (Fig. 5), which is very close to that of a free electron and typical for organic radicals.[58]

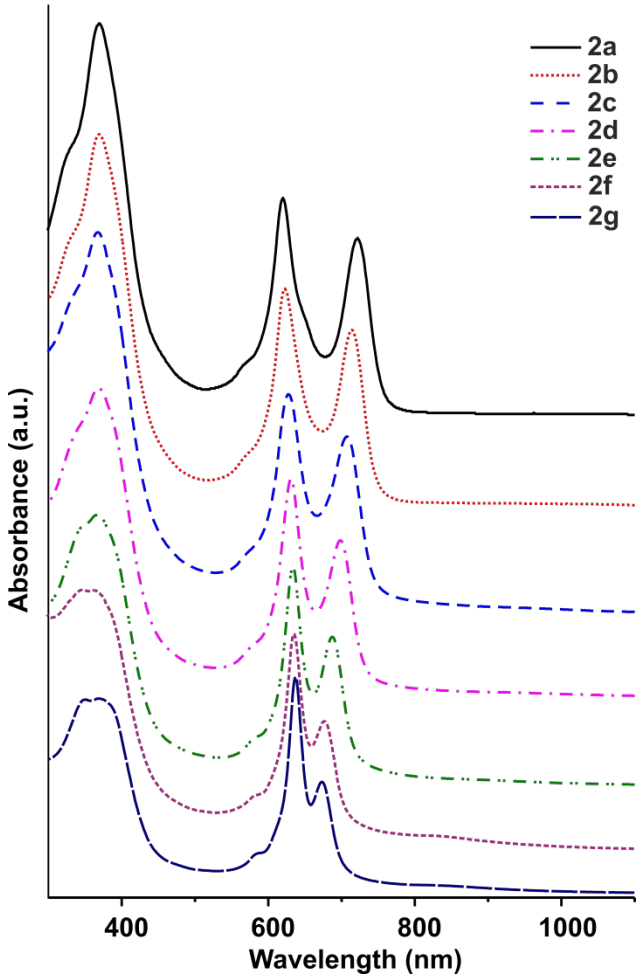

Fig. 3 UV-Vis spectra of reduced forms of complexes **2a–g** in CH_2Cl_2. The spectrum of **2f** is given for the reaction mixture.

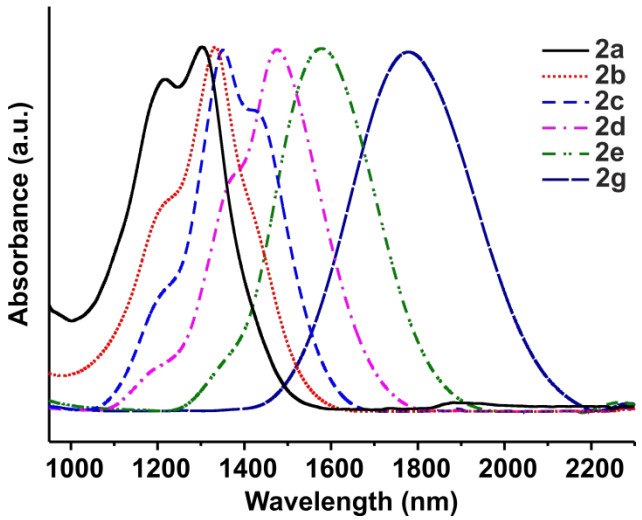

Fig. 4. NIR spectra of neutral forms of **2a–g** in CCl_4.

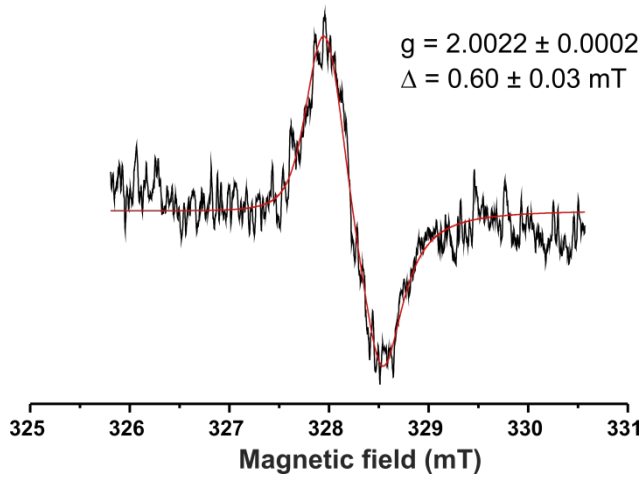

Fig. 5 ESR spectrum of **2g** recorded in toluene at 298 K.

Similarly to bis(Pcs), clear REE size effect on the UV-vis-NIR spectra of **2a–g** can be observed; along with increasing the ionic radius from Lu (**2a**) to La (**2g**), the Q-band splitting values in the anionic form decrease (Fig. 6). In the neutral form, maxima of the Q and IV absorption bands are linearly shifted to the red region of the spectrum, while the opposite tendency is observed in the RV-band region (Fig. 6). These correlations indicate that π-π interactions between the macrocycles become weaker with the increase in REE ionic radius. It is worth noting that splitting of the Q-band in the anionic forms of $[^{t\text{BuPh}}\text{DzPz}]_2\text{Ln}$ is more pronounced than that of Pc_2Ln,[55] which is consistent with stronger interactions between the macrocycles in tetradiazepinoporphyrazine lanthanide double-deckers as discussed above. Moreover, the observed hypsochromic shift of the IV-band in **2g** relative to lanthanum bis(Pcs)[55, 59] by about 350 nm is also consistent with a stronger interligand interactions in $[^{t\text{BuPh}}\text{DzPz}]_2\text{Ln}$.

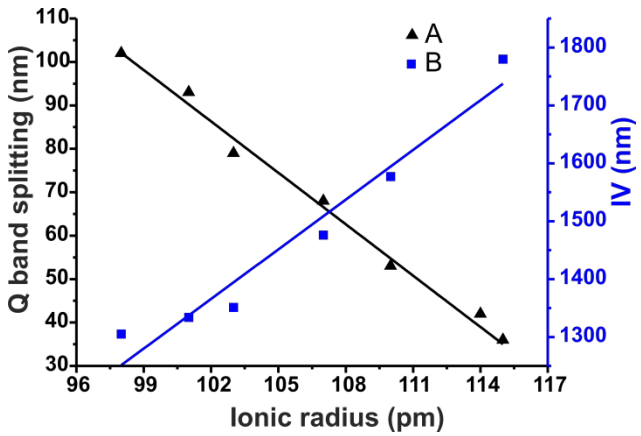

Fig. 6 Plots of Q-band splitting in reduced state (A) and IV in neutral state (B) *versus* the Ln^{III} ionic radius[60] for **2a–g**.

MCD

Figure 7 shows the electronic absorption and magnetic circular dichroism (MCD) spectra of compounds in this study. They can be interpreted using the knowledge accumulated on tetraazaporphyrinoids to date. Compound **1** is a metal-free porphyrazine containing seven-membered 1,4-diazepine rings consisting of two nitrogen atoms and three double bonds. It showed a split Q-band with maxima at 680 (Q_x) and 633 (Q_y) nm and the Soret band at 362 nm. Compared with those of metal-free tetrapyrazinoporphyrazine which shows Q-bands at 648 (Q_x) and 612 (Q_y) nm and the Soret band at 335 nm[61], both bands are shifted to the red by ca. 20–30 nm. This can be interpreted as a practical expansion of the π-system, as seen on going from classical Pcs to Pc analogues with seven-membered rings fused to the porphyrazine core instead of the benzene rings in Pcs.[62] The MCD spectrum of this compound is a superimposition of Faraday B-terms that can be observed when there is no degeneracy in both ground and excited states. Corresponding to the Q_x- and Q_y- bands, negative and positive envelopes were observed, respectively.

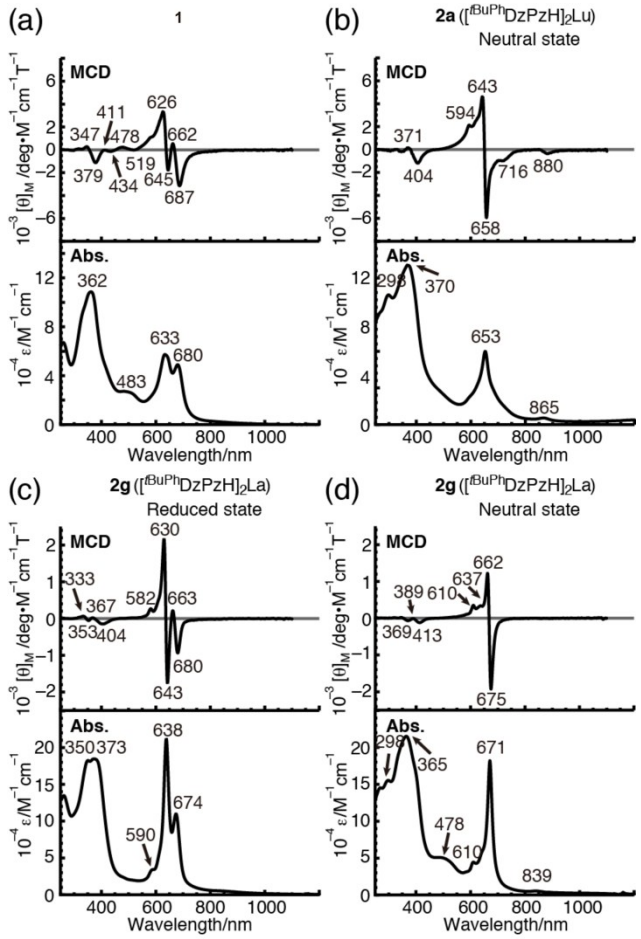

Fig. 7 UV-Vis and MCD spectra of compounds **1**, **2a** and **2g** in CH_2Cl_2.

The neutral forms of $[^{t\text{BuPh}}\text{DzPz}]_2\text{Lu}$ (**2a**) and $[^{t\text{BuPh}}\text{DzPz}]_2\text{La}$ (**2g**) are π-radical species. The spectra of these compounds can be interpreted based on the knowledge of porphyrin or Pc sandwich compounds containing these Ln ions.[63] In the region beyond 600 nm, **2a** showed two peaks at 653 and 865 nm (Fig. 7b), while **2g** showed these peaks at 671 and 839 nm (Fig. 7d). Namely, going from **2a** containing the smaller Lu ion to **2g** containing the larger La ion, the 865 nm band is blue-shifted to 839 nm while the 653 nm band is red-shifted to 671 nm. Judging by the changes in the position of these bands, the small negative MCD envelope corresponding to the 865 and 839 nm absorption bands, and the intense Faraday A-terms associated with the 653 and 671 nm bands, the 865 and 839 nm bands can be assigned to a transition from the singly occupied molecular orbital (SOMO) to the lowest unoccupied molecular orbital (LUMO), and 653 and 671 nm bands to that from the highest occupied molecular orbital (HOMO) to LUMO+1.[63]

The spectra of the reduced form of **2g** can be analyzed in the same way as for the reduced form of the tetrapyrazinoporphyrazine sandwich compound containing Lu ion.[64] Distinct differences between the absorption spectra of the neutral species and the reduced species are seen in the Q-band region, i.e. the reduced species alone shows a clearly split Q-band. The Q-band splitting of the reduced form of **2g** is

only 36 nm (840 cm^{-1}) compared with 102 nm (2280 cm^{-1}) of **2a** and 108 nm (2750 cm^{-1}) of the tetrapyrazinoporphyrazine sandwich compound containing the Lu ion[64] due to the larger ionic radius of La than Lu. According to the molecular orbital (MO) calculation on the reduced forms of the lanthanide sandwich Pc compounds by the valence effective Hamiltonian approach[65], the Q-bands at longer and shorter wavelengths correspond to transitions from a_2 to e_1 and b_1 to e_3 orbitals, respectively, under D_{4d} symmetry, i.e. the excited state is doubly degenerate. In agreement with these assignments, the MCD spectrum showed Faraday A terms corresponding to these split Q-bands. This further indicates that the angular momentum change is distributed to the split bands.

Self-assembly

As mentioned above, the reduced form of **2** can easily be converted to the neutral one by the action of oxidants. Furthermore, we have found that the UV-vis spectrum of the neutral form obtained in the system I_2/CH_2Cl_2 undergoes changes over 2 hours mainly in the area of the hypsochromic shoulder of the Q-band; this implies the predominant formation of H-type aggregates in solution (Fig. 8). Interestingly, the rate of this process increases with an increase in the ionic radius of REE. Addition of a reducing agent to the resulting solution leads to a full regeneration of the initial reduced form indicating that oxidation conditions are nondestructive for the double-decker molecules and the corresponding UV-vis changes are indeed due to the formation of H-aggregates. Study of freshly prepared neutral forms of complexes **2a,d,g** in the medium I_2/CH_2Cl_2 using DLS method (Figs. 8, S43, and S44) revealed the formation of nanoparticles with an average hydrodynamic radius (R_h) of about 20 nm, accounting for approximately 30 molecules, given R_h of the molecule of 6.62 Å according to DOSY experiments. The observed aggregation is also accompanied by a significant drop in the ESR signal intensity (Fig. S45); conversion extent to a radical form is only 10% in CH_2Cl_2 solution.

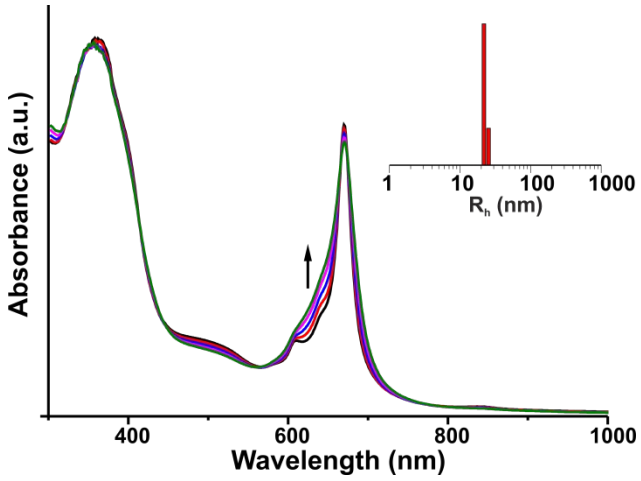

Fig. 8 UV-Vis spectral changes observed during the aggregation of the neutral form of **2g** in CH_2Cl_2. Insert: DLS determined particle size distribution in the resulting solution of **2g** ($C = 1 \cdot 10^{-4}$ M); R_h = 24 nm.

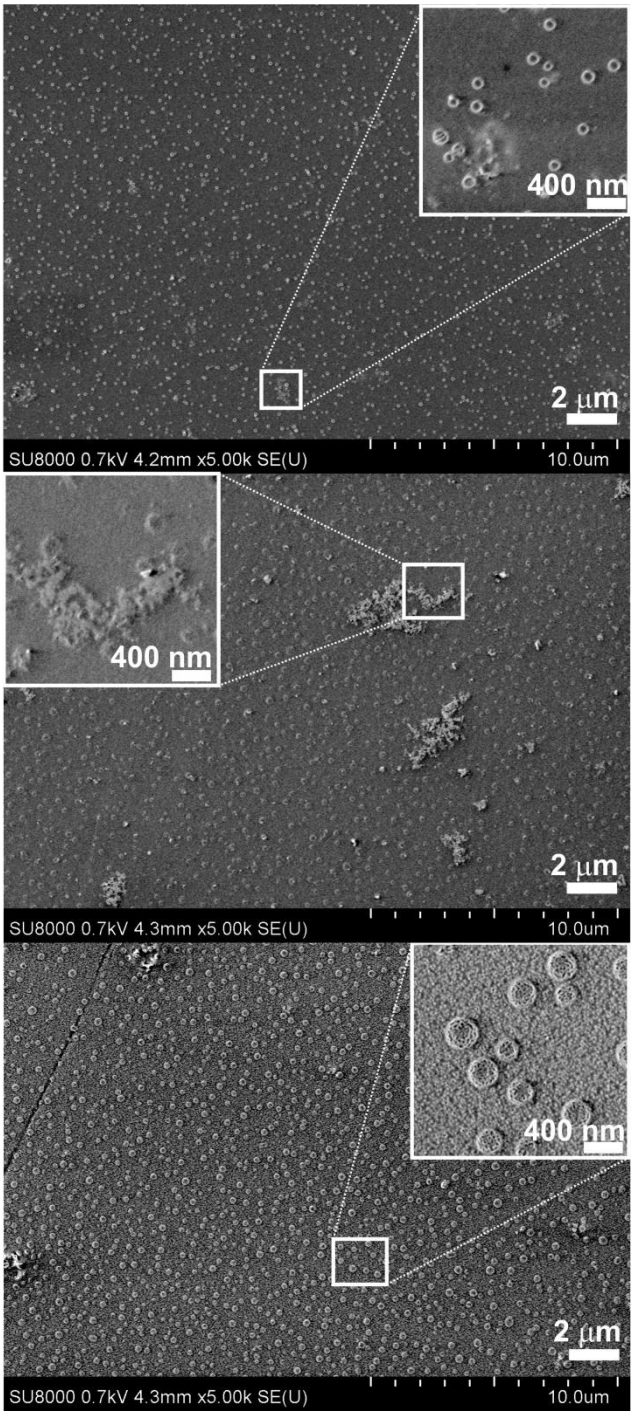

Fig. 9 FE-SEM images of films formed by **2a** (top), **2d** (middle) and **2g** (bottom) compounds.

We assumed that the strong tendency of neutral forms of $[^{tBuPh}DzPz]_2Ln$ to aggregate in solution is due to the possibility of reorientation of the intramolecular hydrogen bonds outwards in the double-decker followed by the formation of intermolecular hydrogen bonds via inversion of diazepine moieties. Thus, weakening of the stabilizing effect of intramolecular hydrogen bonding should alter stability of the neutral forms of **2** making the resulting stability closer to the one of bis(Pcs) and, therefore, should be mainly dependent on

Table 3 Half-wave potentials for **2a–e, 2g** in *o*-DCB

	$E_{1/2}$ (V) vs. SCE [a]								
Compd	L_2Ln^{4-}/L_2Ln^{5-} [b]	L_2Ln^{3-}/L_2Ln^{4-}	L_2Ln^{2-}/L_2Ln^{3-}	L_2Ln^{-}/L_2Ln^{2-}	L_2Ln/L_2Ln^{-}	L_2Ln^{+}/L_2Ln	L_2Ln^{2+}/L_2Ln^{+}	$\Delta E_{1/2}$ [c]	$\Delta E'_{1/2}$ [d]
2a	-1.98	-1.37	-1.06	-0.68	0.34	0.76	-	0.42	1.02
2b	-1.84	-1.35	-1.09	-0.73	0.36	0.79	-	0.43	1.09
2c	-1.87	-1.34	-1.07	-0.71	0.41	0.83	-	0.42	1.12
2d	-1.83	-1.33	-1.05	-0.71	0.41	0.85	-	0.44	1.12
2e	-1.79	-1.31	-1.06	-0.73	0.48	0. 93	-	0.45	1.21
2g	-1.76	-1.38	-1.01	-0.71	0.53	0.98	-	0.45	1.24

[a] $E_{1/2}$ (Fc^+/Fc) = 0.64 V. [b] L = ^{tBuPh}DzPz. [c] $\Delta E_{1/2} = E_{1/2}(L_2Ln^+/L_2Ln) - E_{1/2}(L_2Ln/L_2Ln^-)$. [d] $\Delta E'_{1/2} = E_{1/2}(L_2Ln/L_2Ln^-) - E_{1/2}(L_2Ln^-/L_2Ln^{2-})$.

the strength of the metal-ligand bond. This was confirmed experimentally; in particular, after prolonged storage (for more than 24 hours) of the neutral form of lanthanum compound **2g** in solution, the MALDI-TOF mass spectrum revealed the signal of the free-base ligand **1** in addition to the protonated molecular ion (Fig. S46). In turn, lutetium complex **2a** does not undergo demetallation even after 5 days, which is also confirmed by the MALDI-TOF mass spectrometry data (Fig. S47).

According to the UV-vis data, the reduced forms of **2** reveal no aggregation in solution. Meanwhile, a study of their films using FE-SEM showed dependence of the solid phase morphology on Ln ionic radius. Thus, the films formed are characterized by a grainy texture, with the grain size reaching 30 nm in diameter (Fig. 9). Nanograins, in turn, are able to form more complex structures of spherical shape whose size increases from about 100 to 400 nm going from **2a** to **2g**, respectively. The increased stability of La complex **2g** in reduced form[31] indicates the absence of the tendency to form the intermolecular hydrogen bonds in the solid phase under these conditions. Thus, complexes **2** in their reduced forms tend to exhibit weaker intermolecular interactions, but being anionic in nature they effectively form supramolecular structures through dispersion interactions. Thus, the mechanism of formation of nanostructures based on $[^{tBuPh}DzPz]_2Ln$ is clearly determined by their redox state.

Thermal Analysis

Thermal stability of compounds **2a** and **2g** was studied using thermogravimetry (TG) and differential thermogravimetry (DTG) (Fig. 10). The nearly identical TG-MS results of **2a** and **2g** indicate that nature of REE have no noticeable effect on the complex decomposition behavior. According to evolved gas analysis (mass-spectrometry), the removal of physically adsorbed water takes place until 100 °C (m/z 17 and 18) and thereafter the dehydration of crystalline water occurs (Fig. S48). Under an inert atmosphere (Ar), complexes start to decompose when heated above 300 °C, while decomposition of the complexes in air begins at ca. 250 °C. Results obtained demonstrated sufficiently high thermal stability of double-deckers $[^{tBuPh}DzPz]_2Ln$ comparable to that of substituted REE bis(Pcs).[66, 67] For details please see the Supporting Information.

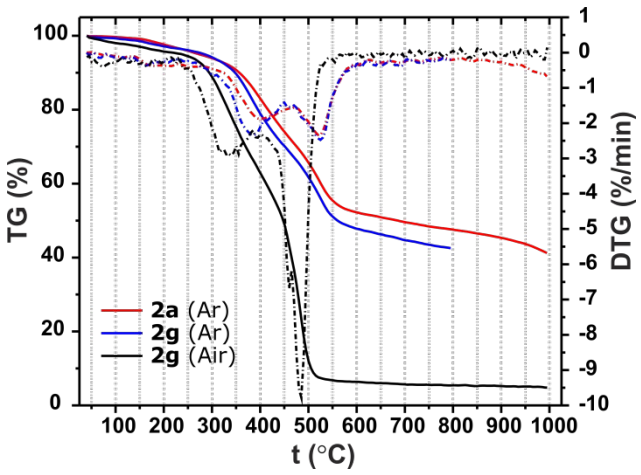

Fig. 10 TG and DTG curves for **2a** and **2g**.

Electrochemistry

The electrochemical properties of complexes **2a–e,g** were measured in *o*-DCB by cyclic voltammetry (CV) and square-wave voltammetry (SWV) at a platinum disk electrode within a potential window from -2.0 to 2.0 V (vs. SCE). Table 3 lists the reduction potentials of the complexes, and Figure 11 depicts representative voltammograms. The pattern of the redox transitions (Figs. 11, S50, and S51) was similar to that of REE bis(Pcs)[54, 56, 68, 69] and included six quasi-reversible ligand-centered processes, which are two one-electron oxidations and four one-electron reductions. It is worth noting that the open circuit potential in the solution of the initial form was in the range of 0.15–0.25 V (vs. SCE), i.e. below the potential of L_2Ln/L_2Ln^- transition, confirming that the complexes have been isolated in the reduced form. As compared to the corresponding REE bis(Pcs)[68], a significant shift (by an average of 0.25 V) of all reduction potentials to positive values was observed, which agrees with the hypsochromic shift of the IV-band compared to bis(Pcs). The potential shift indicates the strong electron withdrawing nature of the diazepine moieties, which stabilizes the reduced forms of the complexes. The redox transition L_2Ln^{2+}/L_2Ln^+ usually observed for bis(Pcs) was not found for $[^{tBuPh}DzPz]_2Ln$ within the available potential window, most probably due to the anodic shift of the transition beyond 2.0 V (vs. SCE).

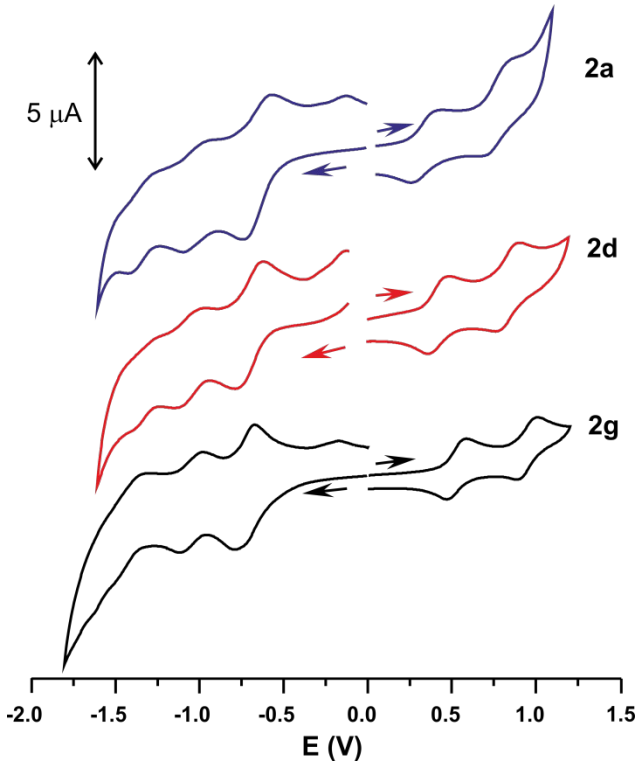

Fig. 11 CV of complexes **2a**, **2d**, **2g** (0.5–1.0 mM, *o*-DCB, 0.15 M $TBABF_4$, scan rate of 0.1 V/s). $E_{1/2}(Fc^+/Fc)$ = 0.64 V.

The value of $\Delta E_{1/2}$ (Table 3) varies in a narrower range (0.42–0.45 V) compared to bis(Pcs) (0.38–0.45 V for *tert*-butyl-substituted complexes[68]), and was higher than that of naphthalocyanines (0.31–0.34 V)[70]. According to the literature [71], such $\Delta E_{1/2}$ values may demonstrate promising semiconducting properties of **2a–g**. The potential difference between the L_2Ln^-/L_2Ln^{2-} and L_2Ln/L_2Ln^- transitions, denoted in Table 3 as $\Delta E'_{1/2}$, corresponds to the HOMO-LUMO gap of the reduced form.[68] The value of $\Delta E'_{1/2}$ increases by 0.22 V in the line from **2a** to **2g**, which agrees with the hypsochromic shift of the Q_2-band (Table 2) and indicates a decrease in the degree of interactions between the macrocycles along with increasing the REE radius. The range of $\Delta E'_{1/2}$ values for the complexes corresponds to that of phthalo- and naphthalocyanines.[68, 70]

Conclusions

A series of sandwich double-decker tetradiazepinoporphyrazine-based lanthanide complexes have been synthesized and characterized using experimental and theoretical methods. According to the TG-MS data the compounds possess sufficiently high thermal stability. Electrochemical studies showed a significant shift of all the potentials towards positive values as compared to the corresponding Pc counterparts, which indicates a strong electron withdrawing nature of diazepine fragments and, therefore, a higher stability of **2a–g** towards oxidation. Using quantum-chemical calculations and NBO analysis we demonstrated for the first time the existence of intermolecular hydrogen bonds provided by the complementarily arranged diazepine fragments in the tetradiazepinoporphyrazine ligand. Thus, the introduction of diazepine heterocycles into the porphyrazine macrocycle leads to the appearance of additional interligand interactions, namely hydrogen bonding, which facilitates the formation of double-decker compounds **2a–g** compared to REE bis(Pcs) and stabilizes the corresponding early lanthanide double-decker complexes towards dissociation. The possibility of reorienting the intramolecular hydrogen bonds outwards in the double-decker via inversion of diazepine moieties promotes aggregation of the complexes. The mechanism of aggregation is shown to be dependent on the redox state of the compound. The specific interactions involving diazepine heterocycles allow us to offer sandwich tetradiazepinoporphyrazine-based lanthanide complexes as promising blocks for the creation of ordered supramolecular architectures. Owing to the fixed mutual orientation of the decks with rotation angle close to 45°, double-deckers **2a–g** represent promising materials for single-molecule magnet studies. Moreover, LIS of H_2O protons in the NMR spectra of paramagnetic complexes **2** make these compounds potentially attractive as magnetic resonance contrast agents.

Acknowledgements

We thank Dr Alexander V. Chernyak for recording the NMR spectra and Alexander V. Zhilenkov for assistance with the DLS experiments. Electron microscopy characterization was performed in the Department of Structural Studies of Zelinsky Institute of Organic Chemistry, Moscow. Financial support from the Russian Foundation for Basic Research (Grant Nos. 16-33-00097, 15-33-21012, 15-03-05890) is gratefully acknowledged. The authors also acknowledge partial support from the M.V. Lomonosov Moscow State University Program of Development.

Notes and references

‡ Present Address: Faculty of Textile Science and Technology, Shinshu University, Tokida, Ueda, 386-8567, Japan

1 Phthalocyanines: Properties and Applications, VCH Publishers, New York, 1989, 1993, 1996.
2 in The Porphyrin Handbook, eds. K. M. Kadish, K. M. Smith and R. Guilard, Academic Press, 2003, vol. 17, pp. 1-285.
3 in The Porphyrin Handbook, eds. K. M. Kadish, K. M. Smith and R. Guilard, Academic Press, 2003, vol. 19, pp. 1-189.
4 in Handbook of Porphyrin Science, eds. K. M. Kadish, K. M. Smith and R. Guilard, World Scientific, Singapore, 2010, vol. 4, pp. 1-441.
5 M. P. Donzello, C. Ercolani, P. A. Stuzhin, A. Chiesi-Villa and C. Rizzoli, Eur. J. Inorg. Chem., 1999, 2075-2084.
6 S. Angeloni and C. Ercolani, J. Porphyrins Phthalocyanines, 2000, 4, 474-483.
7 M. P. Donzello, D. Dini, G. D'Arcangelo, C. Ercolani, R. Zhan, Z. Ou, P. A. Stuzhin and K. M. Kadish, J. Am. Chem. Soc., 2003, 125, 14190-14204.
8 M. P. Donzello, C. Ercolani, L. Mannina, E. Viola, A. Bubnova, O. G. Khelevina and P. A. Stuzhin, Aust. J. Chem., 2008, 61, 262-272.

9 T. Goslinski, J. Piskorz, D. Brudnicki, A. J. P. White, M. Gdaniec, W. Szczolko and E. Tykarska, Polyhedron, 2011, 30, 1004-1011.
10 J. Piskorz, E. Tykarska, M. Gdaniec, T. Goslinski and J. Mielcarek, Inorg. Chem. Commun., 2012, 20, 13-17.
11 P. A. Tarakanov, M. P. Donzello, O. I. Koifman and P. A. Stuzhin, Macroheterocycles 2011, 4(3), 177-183
12 P. A. Stuzhin, P. Tarakanov, S. Shiryaeva, A. Zimenkova, O. I. Koifman, E. Viola, M. P. Donzello and C. Ercolani, J. Porphyrins Phthalocyanines, 2012, 16, 968-976.
13 P. A. Tarakanov, A. O. Simakov, A. Y. Tolbin, I. O. Balashova, V. I. Shestov and L. G. Tomilova, Spectrochim. Acta, Part A, 2015, 139, 464-470.
14 Y. Bian, Y. Zhang, Z. Ou and J. Jiang, in Handbook of Porphyrin Science, eds. K. M. Kadish, K. M. Smith and R. Guilard, World Scientific, Singapore, 2011, vol. 14, pp. 249-460.
15 J. Jiang, K. Kasuga and D. P. Arnold, in Supramolecular Photosensitive and Electroactive Materials, ed. H. S. Nalwa, Academic Press, San Diego, 2001, pp. 113-210.
16 J. Jiang and D. K. P. Ng, Acc. Chem. Res., 2008, 42, 79-88.
17 N. Kobayashi, Coord. Chem. Rev., 2002, 227, 129-152.
18 M. Bouvet, P. Gaudillat and J.-M. Suisse, J. Porphyrins Phthalocyanines, 2013, 17, 628-635.
19 A. B. Karpo, V. E. Pushkarev, V. I. Krasovskii and L. G. Tomilova, Chem. Phys. Lett., 2012, 554, 155-158.
20 A. B. Karpo, A. V. Zasedatelev, V. E. Pushkarev, V. I. Krasovskii and L. G. Tomilova, Chem. Phys. Lett., 2013, 585, 153-156.
21 S. Casilli, M. De Luca, C. Apetrei, V. Parra, Á. A. Arrieta, L. Valli, J. Jiang, M. L. Rodríguez-Méndez and J. A. De Saja, Appl. Surf. Sci., 2005, 246, 304-312.
22 M. L. Rodriguez-Méndez, M. Gay and J. A. de Saja, J. Porphyrins Phthalocyanines, 2009, 13, 1159-1167.
23 K. Katoh, Y. Yoshida, M. Yamashita, H. Miyasaka, B. K. Breedlove, T. Kajiwara, S. Takaishi, N. Ishikawa, H. Isshiki, Y. F. Zhang, T. Komeda, M. Yamagishi and J. Takeya, J. Am. Chem. Soc., 2009, 131, 9967-9976.
24 X. Kong, X. Zhang, D. Gao, D. Qi, Y. Chen and J. Jiang, Chem. Sci., 2015, 6, 1967-1972.
25 Y.-S. Fu, J. Schwöbel, S.-W. Hla, A. Dilullo, G. Hoffmann, S. Klyatskaya, M. Ruben and R. Wiesendanger, Nano Lett., 2012, 12, 3931-3935.
26 H. Wang, K. Qian, D. Qi, W. Cao, K. Wang, S. Gao and J. Jiang, Chem. Sci., 2014, 5, 3214-3220.
27 M. Gonidec, D. B. Amabilino and J. Veciana, Dalton Trans., 2012, 41, 13632-13639.
28 N. L. Bill, O. Trukhina, J. L. Sessler and T. Torres, Chem. Commun., 2015.
29 D. N. Woodruff, R. E. P. Winpenny and R. A. Layfield, Chem. Rev., 2013, 113, 5110-5148.
30 E. N. Tarakanova, P. A. Tarakanov, V. E. Pushkarev and L. G. Tomilova, J. Porphyrins Phthalocyanines, 2013, 18, 149-154.
31 E. N. Tarakanova, S. A. Trashin, P. A. Tarakanov, V. E. Pushkarev and L. G. Tomilova, Dyes Pigm., 2015, 117, 61-63.
32 E. N. Tarakanova, O. A. Levitskiy, T. V. Magdesieva, P. A. Tarakanov, V. E. Pushkarev and L. G. Tomilova, New J. Chem., 2015, 39, 5797-5804.
33 J. G. Stites, C. N. McCarty and L. L. Quill, J. Am. Chem.Soc., 1948, 70, 3142-3143.
34 V. V. Kachala, L. L. Khemchyan, A. S. Kashin, N. V. Orlov, A. A. Grachev, S. S. Zalesskiy and V. P. Ananikov, Russ. Chem. Rev., 2013, 648 - 685.
35 A. S. Kashin and V. P. Ananikov, Russ. Chem. Bull. Int. Ed., 2011, 60, 2602 - 2607.
36 F. Neese, Wiley Interdiscip. Rev.: Comput. Mol. Sci., 2012, 2, 73-78.
37 F. Weigend and R. Ahlrichs, Phys. Chem. Chem. Phys., 2005, 7, 3297-3305.
38 X. Cao and M. Dolg, J. Mol. Struct.: THEOCHEM, 2002, 581, 139-147.
39 C. Van Alsenoy, J. Comput. Chem., 1988, 9, 620-626.
40 A. R. Kendall and A. H. Früchtl, Theor. Chem. Acc., 1997, 97, 158-163.
41 F. Weigend, Phys. Chem. Chem. Phys., 2006, 8, 1057-1065.
42 S. Grimme, J. Antony, S. Ehrlich and H. Krieg, J. Chem. Phys., 2010, 132, 154104.
43 S. Grimme, S. Ehrlich and L. Goerigk, J. Comput. Chem., 2011, 32, 1456-1465.
44 E. D. Glendening, C. R. Landis and F. Weinhold, J. Comput. Chem., 2013, 34, 1429-1437.
45 V. E. Pushkarev, M. O. Breusova, E. V. Shulishov and Y. V. Tomilov, Russ. Chem. Bull. Int. Ed., 2005, 54, 2087-2093.
46 G. Clarisse and M. T. Riou, Inorg. Chim. Acta, 1987, 130, 139-144.
47 D. P. Arnold and J. Jiang, J. Phys. Chem. A, 2001, 105, 7525-7533.
48 A. G. Martynov, O. V. Zubareva, Y. G. Gorbunova, S. G. Sakharov, S. E. Nefedov, F. M. Dolgushin and A. Y. Tsivadze, Eur. J. Inorg. Chem., 2007, 4800-4807.
49 P. A. Tarakanov, A. O. Simakov, A. V. Dzuban, V. I. Shestov, E. N. Tarakanova, V. E. Pushkarev and L. G. Tomilova, Org. Biomol. Chem., 2016, 14, 1138-1146.
50 K. Katoh, H. Isshiki, T. Komeda and M. Yamashita, Chem. - Asian J., 2012, 7, 1154-1169.
51 K. Katoh, B. K. Breedlove and M. Yamashita, Chem. Sci., 2016.
52 V. E. Pushkarev , A. Y. Tolbin, F. E. Zhurkin, N. E. Borisova, S. A. Trashin, L. G. Tomilova and N. S. Zefirov Chem. Eur. J., 2012, 18, 9046-9055.
53 T. V. Dubinina, K. V. Paramonova, S. A. Trashin, N. E. Borisova, L. G. Tomilova and N. S. Zefirov, Dalton Trans., 2014, 43, 2799-2809.
54 I. Yilmaz, T. Nakanishi, A. Gürek and K. M. Kadish, J. Porphyrins Phthalocyanines, 2003, 7, 227-238.
55 F.-L. Lu, Polyhedron, 2007, 26, 3939-3946.
56 V. E. Pushkarev , A. Y. Tolbin, F. E. Zhurkin, N. E. Borisova, S. A. Trashin, L. G. Tomilova and N. S. Zefirov Chem. - Eur. J., 2012, 18, 9046-9055.
57 I. V. Zhukov, V. E. Pushkarev, L. G. Tomilova and N. S. Zefirov, Russ. Chem. Bull. Int. Ed., 2005, 54, 189-194.
58 J.-J. Andre, K. Holczer, P. Petit, M.-T. Riou, C. Clarisse, R. Even, M. Fourmigue and J. Simon, Chem. Phys. Lett., 1985, 115, 463-466.
59 L. G. Tomilova, E. V. Chernykh, N. A. Ovchinnikova, E. V. Bezlepko, V. M. Mizin and V. A. Lukyanets, Optika I Spectroscopiya, 1991, 70, 775-778.
60 R. Shannon, Acta Crystallographica, Section A, 1976, 32, 751-767.
61 D. Wöhrle, G. Schnurpfeil and G. Knothe, Dyes Pigm., 1992, 18, 91-102.
62 N. Kobayashi, T. Nonomura and K. Nakai, Angew. Chem., Int. Ed., 2001, 40, 1300-1303.
63 A. Muranaka, Y. Matsumoto, M. Uchiyama, J. Jiang, Y. Bian, A. Ceulemans and N. Kobayashi, Inorg. Chem., 2005, 44, 3818-3826.
64 N. Kobayashi, J. Rizhen, S.-i. Nakajima, T. Osa and H. Hino, Chem. Lett., 1993, 22, 185-188.
65 E. Ortí, J. L. Brédas and C. Clarisse, J. Chem. Phys., 1990, 92, 1228-1235.
66 A. G. Gürek, V. Ahsen, D. Luneau and J. Pécaut, Inorg. Chem., 2001, 40, 4793-4797.
67 R. Słota, G. Dyrda, M. Hofer, G. Mele, E. Bloise and R. d. Sole, Molecules, 2012, 17, 10738.
68 P. Zhu, F. Lu, N. Pan, D. P. Arnold, S. Zhang and J. Jiang, Eur. J. Inorg. Chem., 2004, 510-517.

69 V. E. Pushkarev, A. Y. Tolbin, N. E. Borisova, S. A. Trashin and L. G. Tomilova, Eur. J. Inorg. Chem., 2010, 5254-5262.
70 R. Li, X. Zhang, N. Pan, P. Zhu, N. Kobayashi and J. Jiang, J. Porphyrins Phthalocyanines, 2005, 09, 40-46.
71 M. Bouvet and J. Simon, Chem. Phys. Lett., 1990, 172, 299-302.